RSC Advances

COMMUNICATION

View Article Online
View Journal | View Issue

Cite this: *RSC Adv.*, 2014, **4**, 19533

Received 12th March 2014
Accepted 15th April 2014

DOI: 10.1039/c4ra02153c

www.rsc.org/advances

Platinum decorated hierarchical top-porous/bottom-tubular TiO_2 arrays for enhanced gas phase photocatalytic activity

Dandan Yuan,[a] Yang Gao,[a] Hongjun Wu,*[a] Tongxin Xiao,[a] Yang Wang,[a] Baohui Wang[a] and Zhonghai Zhang*[b]

In this communication, Pt nanoparticles (NPs) were successfully loaded on hierarchical TiO_2 nanotube arrays (TiO_2 NTs) for efficient decomposition of gas phase pollutants. The loading of Pt NPs on TiO_2 NTs significantly enhanced the photocatalytic activity due to reduction of the recombination of photogenerated electrons and holes.

Photocatalytic technology has received significant attention as a promising way for remediating experimental pollution, and lots of materials, especially metal oxide semiconductors, have been widely explored as photocatalysts.[1–3] Among them, titanium dioxide (TiO_2) is regarded as one of the most popular photocatalysts owing to its high resistance to photo-corrosion, physical and chemical stability, ease of availability and low cost.[4–6] Notably, TiO_2 nanotube arrays (TiO_2 NTs), fabricated by electrochemical anodization method, have been demonstrated to be the most efficient photocatalysts for environmental protection and solar energy conversion because of their unique morphological and electronic properties, especially their monodirectional electron transfer, high electron mobility, and enhanced light absorption induced by their one-dimensional nanostructure.[7–9] In this communication, more interestingly, the hierarchical TiO_2 NTs with top-porous and bottom-tubular structures, fabricated by a two-step anodization method, were rationally selected as photocatalyst as it has been proven better photocatalytic activity than conventional TiO_2 NTs due to its higher uniformity and enhanced light scattering activity.[10]

For further enhancing photocatalytic activity of TiO_2 NTs, noble metal nanoparticle decoration was an effective option. Many noble metals were investigated to couple with TiO_2, including Au,[11,12] Ag,[13] Pd,[14] and Ru.[15] In this communication, Pt nanoparticles (NPs) were selected due to its higher work function (5.65 eV), which would be more favorable for formation a Schottky junction with TiO_2.[16] As the electron affinity of anatase TiO_2 (~4.2 eV) is significantly lower than the work function of Pt, the higher work function will induce higher electronic potential between Pt and TiO_2, which accelerates the electron transfer and reduces the electron–hole recombination. Even the photocatalytic studies on TiO_2 with/without Pt NPs have been extensively studied, however, previous studies were focused on photocatalytic activity in aqueous solution,[17–20] the photocatalytic activity in gas phase has rarely studied. To our best knowledge, the gas phase photocatalytic activity of noble metal decorated hierarchical TiO_2 NTs has not been reported. In this study, the gas phase photocatalytic activity of TiO_2 NTs and Pt/TiO_2 NTs were estimated by decomposition of evaporated methanol.

The hierarchical TiO_2 NTs were fabricated by a two-step anodization process (Scheme 1(a)–(d)). Prior to anodization, the Ti sheets were first degreased by sonicating in ethanol and cold distilled water, followed by drying in pure nitrogen stream. The anodization was carried out using a conventional two-electrode system with the Ti sheet as an anode and a Pt gauze (Aldrich, 100 mesh) as a cathode respectively. All electrolytes consisted of 0.5 wt% NH_4F in ethylene glycol (EG) solution with 2 vol%

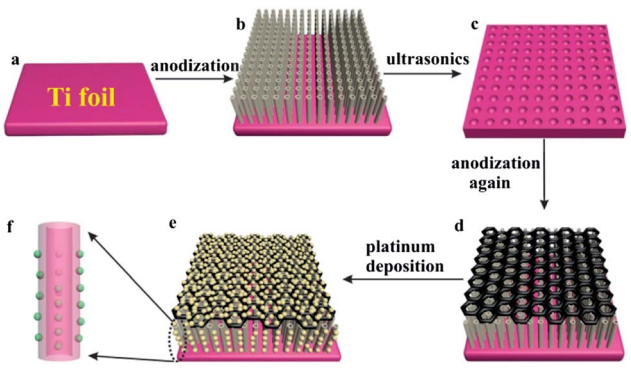

Scheme 1 Two-step anodization processes for fabrication of hierarchical TiO_2 NTs and photocatalytic reduction for decoration of Pt NPs.

[a]*Provincial Key Laboratory of Oil & Gas Chemical Technology, College of Chemistry & Chemical Engineering, Northeast Petroleum University, Daqing 163318, China. E-mail: hjwu1979@gmail.com*

[b]*Department of Chemistry, East China Normal University, 500 Dongchuan Road, Shanghai 200241, China. E-mail: zhzhang@chem.ecnu.edu.cn*

water. All the anodization experiments were carried out at room temperature. In the first-step anodization, the Ti sheet was anodized at 50 V for 30 min, then the as-grown nanotube layer was ultrasonically removed in deionized water, leaving compact two-dimensional hexagonal pattern on the surface of the Ti sheet alone. The patterned Ti sheet then underwent the second anodization at 20 V for 30 min, in which the hexagonal pattern formed top-porous structure and subjective NTs grew below the top-porous layer. After second-step anodization, the prepared TiO_2 NTs sample was cleaned with distilled water and dried off with N_2 gas. The as-anodized TiO_2 NTs were annealed in air at 450 °C for 1 h with a heating rate of 5 °C min^{-1}.

The Pt NPs were decorated on the TiO_2 NTs by a photocatalytic reduction method using platinum(II) acetylacetonate ($Pt(AcAc)_2$) as a precursor (Scheme 1(e) and (f)). The $Pt(AcAc)_2$ was diluted in deionized water and ethanol with a water–ethanol volume ratio of 10 : 1, and the concentration of $Pt(AcAc)_2$ was fixed at 1 mM. The Ti sheet containing the prepared TiO_2 NTs were soaked into the Pt precursor solution for 24 h, then rinsed with deionized water, and subsequently irradiated with simulated solar light for 30 min.

The morphology of nanotubular structures and distribution of nanoparticles were determined by filed-emission scanning electron microscope (FESEM, Zeiss SigmaHV) and transmission electron microscope (TEM, Tecnai T12). Fig. 1a shows a top view SEM image of TiO_2 NTs. An individual top hexagonally porous structure is fairly observed, with an average diameter of the hexagonal pores about 200 nm and a wall-thickness of 19 nm. A cross-sectional view of the TiO_2 NTs is presented in the bottom-left inset of Fig. 1a, indicates a corresponding tubular structure with a length of ~600 nm. Fig. 1b is a high-magnification top-view SEM image of Pt/TiO_2 NTs, which shows the Pt NPs are homogeneously decorated on the top porous TiO_2 structure with average diameter of ~20 nm. The TEM image of Pt/TiO_2 NTs is presented in the inset of Fig. 1b, which clearly showed Pt NPs are not only decorated on the outer side of NT but also into the inter side of NTs with same diameter size of 20 nm as shown in SEM image.

The crystal structures were characterized by grazing incidence X-ray diffraction (GIXRD) analysis by an X-ray diffractometer (Rigaku D/MAX-2200) with Cu Kα source in the range of $2\theta = 20$–$70°$. The XRD patterns of the hierarchical TiO_2 NTs and Pt/TiO_2 NTs are shown in Fig. 1c. Clearly, both of them presented pure crystalline anatase with strong preferential orientation of (101). In addition, the Pt/TiO_2 NTs sample shows an extra Pt XRD pattern with strong orientation of (111), which implies that the Pt NPs are successfully doped on the TiO_2 NTs.

The chemical compositions of Pt/TiO_2 NTs were analyzed by energy dispersive spectrometer (EDS) equipped with FESEM. The EDS spectra in Fig. 1d showed another evidence for Pt existence on the TiO_2 NTs, and the Pt showed an atomic ratio of 0.92% in the Pt/TiO_2 NTs composites.

The X-ray photoelectron spectra (XPS) were recorded to determine the chemical components and the valence state of Pt on the surface of the Pt/TiO_2 NTs. The XPS data were collected by an Axis Ultra instrument (Kratos Analytical) under ultrahigh vacuum (<10^{-8} Torr) and by using a monochromatic Al Kα X-ray

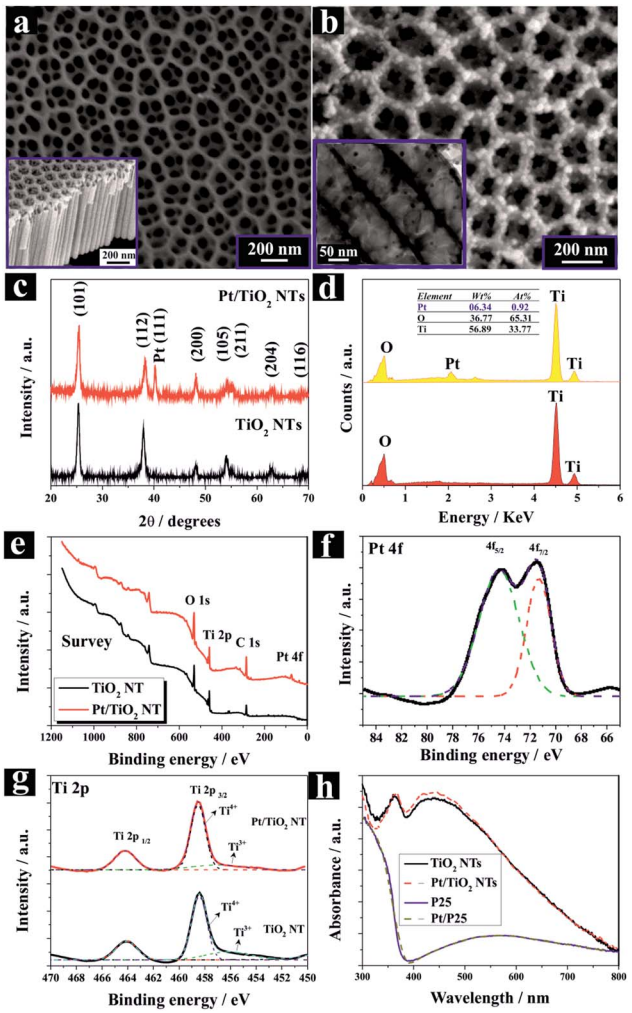

Fig. 1 (a) Top-view SEM image of hierarchical TiO_2 NTs, the bottom left inset presents cross-sectional view SEM image; (b) top-view SEM image of Pt/TiO_2 NTs, the inset shows the TEM image of Pt NTs inside the TiO_2 NTs; (c) XRD patterns of TiO_2 NTs and Pt/TiO_2 NTs; (d) EDS spectra of Pt/TiO_2 NTs (the top/yellow one) and TiO_2 NTs (the bottom/red one); (e) XPS survey; (f) core-level spectrum of Pt 4f of Pt/TiO_2 NTs; (g) core-level XPS of Ti 2p; and (h) diffuse reflectance UV-vis absorption spectra of TiO_2 NTs, Pt/TiO_2 NTs, P25 TiO_2 NPs and Pt/P25 TiO_2 NPs.

source operating at 150 W. The survey and high-resolution spectra were collected at fixed analyzer pass energies of 160 and 20 eV, respectively. Binding energies were referenced to the C1s binding energy of adventitious carbon contamination which was taken to be 285.0 eV. As shown in Fig. 1e, the surface of the TiO_2 NTs and Pt/TiO_2 NTs both contained Ti, O, and C elements, but an additional Pt peak was observed in the survey of Pt/TiO_2 NTs. The core-level XPS spectrum of Pt, shown in Fig. 1f, confirmed the existence of metallic Pt on the surface. The core-level XPS spectra of Ti 2p in Fig. 1g shows doublet peaks at 458.4 and 464.1 eV,[21] corresponding to the Ti $2p_{3/2}$ and Ti $2p_{1/2}$, respectively. Furthermore, a peak at 455.7 eV has been defined as Ti^{3+} both in TiO_2 NTs and Pt/TiO_2 NTs, but showed much higher intensity on TiO_2 NTs than in Pt/TiO_2 NTs. The decreased intensity of Ti^{3+} on Pt/TiO_2 NTs can be ascribed to the

electron transfer from TiO_2 to Pt as the formation of Schottky junction.[22]

Optical absorption is important factor for the PC performance on TiO_2 materials. The diffuse reflectance UV-vis absorption spectra were employed to characterize the optical absorption properties TiO_2 NTs, Pt/TiO_2 NTs, P25 TiO_2 NPs and Pt/P25 TiO_2 NPs (Fig. 1h). The light in UV region can be absorbed because its photons own higher energy than the band gap of TiO_2, while the TiO_2 NTs sample showed much stronger light absorption in visible light region than P25 TiO_2 NPs sample, which can be ascribed to the unique hierarchical structure of TiO_2 NTs, induced strong light scattering. After Pt NPs loading, the both of Pt/TiO_2 NTs and Pt/P25 TiO_2 NPs samples did not show significant difference to their pristine samples.

The gas phase photocatalytic activities of TiO_2 NTs and Pt/TiO_2 NTs were estimated by decomposition of evaluated methanol (5 μL). The concentration of methanol and corresponding degraded by-products were measured by Fourier transform infrared (FTIR) spectroscopy (Bruker Tensor27). All the photocatalytic measurements were performed in a homemade cylindrical cell with 5 cm length and 3.6 cm width, in which the TiO_2 NT and Pt/TiO_2 NT samples were contained respectively. The photocatalytic degradation of methanol was carried out under irradiation with simulated solar light with intensity of 100 mW cm^{-2} (model SET-140F, Seric LTD) with an infrared blocking filter. Fig. 2a and b shows the FTIR spectra of methanol decomposition as a function of irradiation time on TiO_2 NTs and Pt/TiO_2 NTs respectively. Before the illumination, the initial methanol processes the bands at 1031, 1055, 1340, 2860, 2950, and 3685 cm^{-1}, which bands correspond to the C–O stretching, CH_3 rocking, O–H bending, C–H parallel symmetric stretching, C–H out of plane asymmetric stretching, O–H stretching, respectively.[23–26] As the increase of irradiation time, all these bands started to decrease in intensity and new peaks appeared at 669, 1456, 1640, 1750, 2360 and 3440 cm^{-1}. The band at 1456 cm^{-1} can be assigned to the out of plane asymmetric bending of C–H, 1640 cm^{-1} proved the formation of isolated C=C bonds, and 1750 cm^{-1} can be assigned to the C=O stretching vibration modes.[27,28] The gaseous CO_2 is a linear molecule with two infrared active absorption bands at 2360 cm^{-1} (antisymmetric stretching mode) and 669 cm^{-1} (bending mode).[29,30] Hence, one can conclude that the primary two peaks centered at 2360 and 669 cm^{-1} imply the formation of CO_2 gas when methanol is decomposed. In the end, after 60 min, just CO_2 and H_2O (3440 cm^{-1}) existence as the results of completed decomposition of methanol on the Pt/TiO_2 NTs sample.

Based on the photocatalytic experimental data, we summarized the CO_2 transmittance peak height (2360 cm^{-1}, CO_2) for TiO_2 NTs and Pt/TiO_2 NTs respectively in Fig. 3a. In addition, for comparing the photocatalytic activity of our TiO_2 NTs samples with commercial available photocatalyst, P25 TiO_2 NPs based photocatalytic films, with similar thickness of TiO_2 NTs, were also prepared on same Ti substrates and loaded Pt NPs with same method. The photocatalytic data of CO_2 transmittance peak height on TiO_2 NPs and Pt/TiO_2 NPs were also presented in

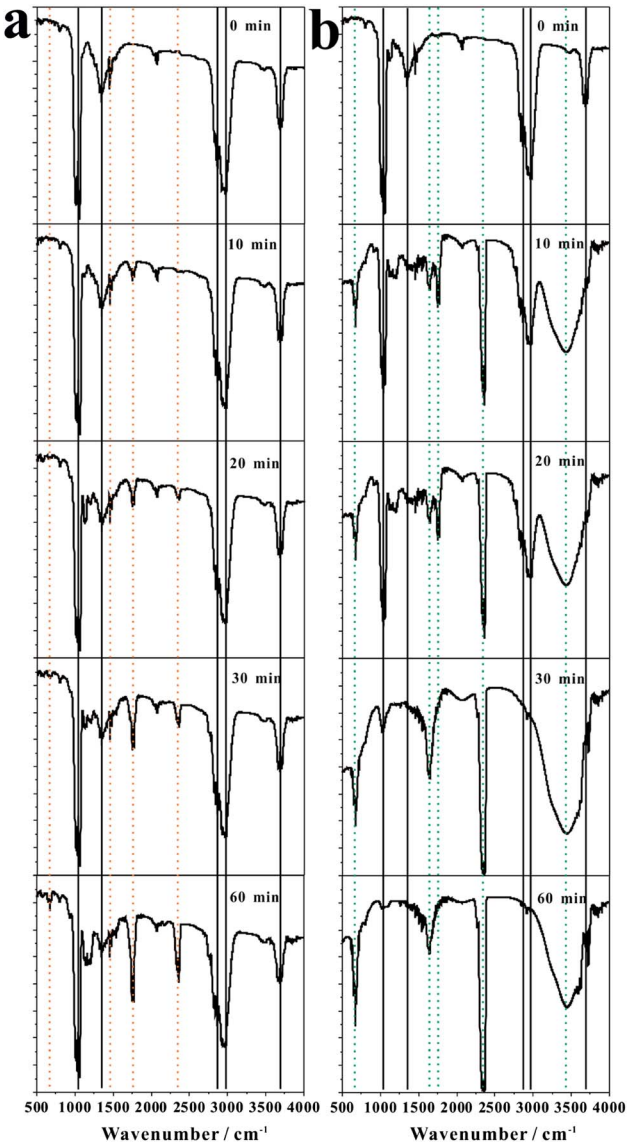

Fig. 2 Decomposition of methanol on TiO_2 NTs (a) and Pt/TiO_2 NTs (b) respectively as a function of irradiation time.

Fig. 3a. The experimental data of Fig. 3a were found to fit approximately a pseudo-first-order kinetic model by the linear transforms $f(t) = f_{inf}[1 - \exp(-kt)]$ (f is peak height, f_{inf} is peak height at infinite time, and k is rate constant).[31] The corresponding curves were presented in Fig. 3b, and the values of rate constant, k, were also showed in Fig. 3b. Clearly, the Pt/TiO_2 NTs showed the highest k value, and our TiO_2 NTs sample showed higher k value than TiO_2 NPs but lower the Pt/TiO_2 NPs. The enhanced photocatalytic activity after Pt deposition may be ascribed the possible formation of Schottky-junction between Pt NPs and TiO_2 NTs. Fig. 3c presented the stability of Pt/TiO_2 NTs during multiple cycles for methanol decomposition. Clearly, after five cycles, the Pt/TiO_2 NTs did not exhibit any significant loss of their PC activities, indicating their high stability under operation conditions, which is important for practical applications.

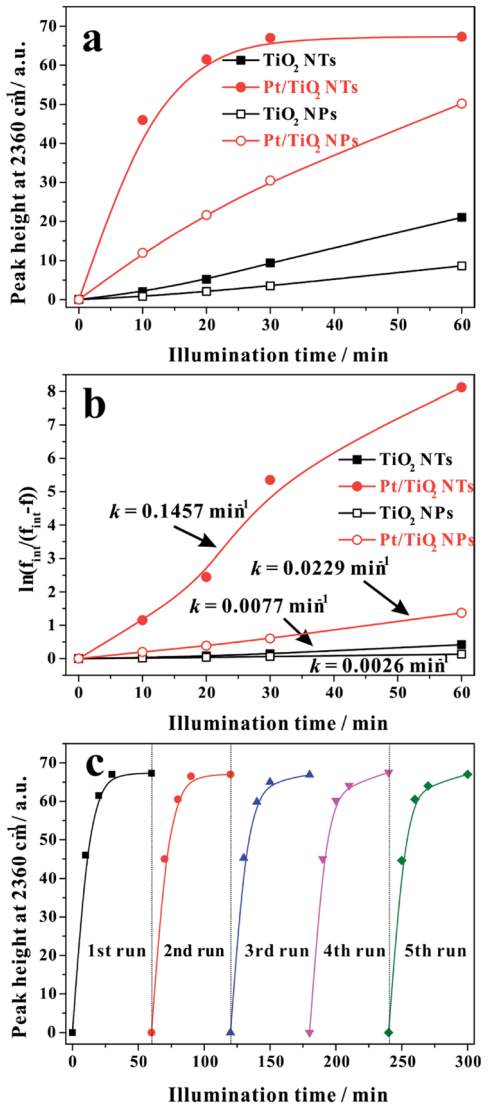

Fig. 3 (a) Variation of the peak height of 2360 cm^{-1} corresponding to the normal vibration of CO_2 molecules derived from the FTIR transmittance spectra with the irradiation time; (b) comparison performance of constant k on TiO_2 NPs, TiO_2 NTs, Pt/TiO_2 NPs and Pt/TiO_2 NTs respectively; (c) stability of Pt/TiO_2 NTs for methanol decomposition.

The gas phase photocatalytic mechanism was also discussed here. As illuminated with energy higher than the band gap of TiO_2, electrons (e^-) on valence band will be excited to the conduction band, at the same time in the valence band a positively charged hole (h^+) is produced, those electron–holes generated after excitation move quickly to surface from inside and the electrons will transfer to Pt through the Schottky interface of TiO_2 and Pt. Under the condition of photocatalytic oxidation on methanol, the oxygen adsorbing on the surface of the catalyst was reduced to $^{\bullet}O_2^-$ by photoelectrons on TiO_2 and Pt surface, and trace water is oxidized to $^{\bullet}OH$ by such holes on TiO_2, which both provide highly active oxidant for the methanol oxidation. The $^{\bullet}O_2^-$ and $^{\bullet}OH$ radicals attack C–H bond in methanol, and then with lively hydrogen atoms to form new free radicals, which stimulates chain reaction, and first oxidation is to form aldehyde then to formic acid, and then ultimately make methanol deeply decompose to H_2O and CO_2. The reaction process is shown below:

$$TiO_2 + h\nu \rightarrow e^- + h^+ \quad (1)$$

$$e^- + Pt \rightarrow Pt^- \quad (2)$$

$$e^- + O_2 \rightarrow {}^{\bullet}O_2^- \quad (3)$$

$$Pt^- + O_2 \rightarrow {}^{\bullet}O_2^- \quad (4)$$

$$H_2O + h^+ \rightarrow {}^{\bullet}OH + H^+ \quad (5)$$

$$CH_3OH + {}^{\bullet}OH \rightarrow {}^{\bullet}CH_2OH + H_2O \quad (6)$$

$$2CH_3OH + 2h^+ \rightarrow {}^{\bullet}CH_2OH + {}^{\bullet}CH_3 + H_2O \quad (7)$$

$${}^{\bullet}CH_2OH + {}^{\bullet}O_2^- \rightarrow HCHO + {}^{\bullet}OOH^- \rightarrow HCOOH + OH^- \quad (8)$$

$$HCOOH + h^+ \rightarrow CO_2 + 2H^+ \quad (9)$$

$$H^+ + OH^- \rightarrow H_2O \quad (10)$$

In summary, Pt NPs decorated hierarchical TiO_2 NTs were successfully designed and estimated of gas phase photocatalytic activity. It had been revealed that Pt modified the inherent properties of TiO_2 NTs as well as affected the photocatalytic activity. The Pt/TiO_2 NTs meaningfully proved the electron transfer and reduced the recombination of photoelectrons and holes. Compared with the pure TiO_2 NT electrode, the Pt/TiO_2 NT electrode showed an outstanding enhancement on photocatalytic decomposition of methanol.

Acknowledgements

H.W. thanks to the support from New Century Excellent Talent Project of the Department of Education, Heilongjiang Province, P. R. China, and Z.Z. thanks to the support from "Yingcai" program of ECNU.

Notes and references

1 X. Chen and S. S. Mao, *Chem. Rev.*, 2007, **107**, 2891.
2 A. Kubacka, M. Fernandez-Garcia and G. Colon, *Chem. Rev.*, 2012, **112**, 1555.
3 J. H. Pan, Z. Lei, W. I. Lee, Z. Xiong, Q. Wang and X. S. Zhao, *Catal. Sci. Technol.*, 2012, **2**, 147.
4 J. Zhang, W. Chen, J. Xi and Z. Ji, *Mater. Lett.*, 2012, **79**, 259.
5 Y. Wang, C. Feng, Z. Jin, J. Zhang, J. Yang and S. Zhang, *J. Mol. Catal. A: Chem.*, 2006, **260**, 1.
6 Y. Wang, K. Yu, H. Yin, C. Song, Z. Zhang, S. Li, H. Shi, Q. Zhang, B. Zhao, Y. Zhang and Z. Zhu, *J. Phys. D: Appl. Phys.*, 2013, **46**, 175303.
7 H. Wu and Z. Zhang, *Int. J. Hydrogen Energy*, 2011, **36**, 13481.
8 H. Wu and Z. Zhang, *J. Solid State Chem.*, 2011, **184**, 3202.
9 G. K. Mor, K. Shankar, M. Paulose, O. K. Varghese and C. A. Grimes, *Nano Lett.*, 2006, **6**, 215.

10 Z. Zhang and P. Wang, *Energy Environ. Sci.*, 2012, **5**, 6506.
11 Z. Zhang, L. Zhang, M. N. Hedhili, H. Zhang and P. Wang, *Nano Lett.*, 2013, **13**, 14.
12 V. Illiev, D. Tomova, L. Bilyaraka and G. Tyuliev, *J. Mol. Catal. A: Chem.*, 2007, **263**, 32.
13 M. S. Lee, S. Hong and M. Mohsen, *J. Mol. Catal. A: Chem.*, 2005, **242**, 135.
14 Z. Zhang, Y. Yu and P. Wang, *ACS Appl. Mater. Interfaces*, 2012, **4**, 990.
15 X. Shen, L. Garces, Y. Ding, K. Laubernds, R. P. Zerger, M. Aindow, E. J. Neth and S. L. Suib, *Appl. Catal., A*, 2008, **335**, 187.
16 W. N. Wang, W. J. An, B. Ramalingam, S. Mukherjee, D. M. Niedzwiedzki, S. Gangopadhyay and P. Biswas, *J. Am. Chem. Soc.*, 2012, **134**, 11276.
17 A. A. Ismail and D. W. Bahnemann, *J. Phys. Chem. C*, 2011, **115**, 5784.
18 Z. Zheng, B. Huang, X. Qin, X. Zhang, Y. Dai and M. H. Whangbo, *J. Mater. Chem.*, 2011, **21**, 9079.
19 X. Feng, J. D. Sloppy, T. J. LaTempa, M. Paulose, S. Komarneni, N. Bao and C. A. Grimes, *J. Mater. Chem.*, 2011, **21**, 13429.
20 Y. Zhang, W. Rong, Y. Fu and X. Ma, *J. Polym. Environ.*, 2011, **19**, 966.
21 B. Liu and H. C. Zeng, *Chem. Mater.*, 2008, **20**, 2711.
22 Z. Zhang, M. N. Hedhili, H. Zhu and P. Wang, *Phys. Chem. Chem. Phys.*, 2013, **15**, 15637.
23 C. Binet and M. Daturi, *Catal. Today*, 2001, **70**, 155.
24 Z. Zhang, M. F. Hossain, T. Arakawa and T. Takahashi, *J. Hazard. Mater.*, 2010, **176**, 973.
25 K. Prabakar, T. Takahashi, T. Nakashima, Y. Kubota and A. Fujishima, *J. Vac. Sci. Technol., A*, 2006, **24**, 1613.
26 K. Mudalige, S. Warren and M. Trenary, *J. Phys. Chem. B*, 2000, **104**, 2448.
27 C. S. Colley, S. G. Kazarian and P. D. Weinberg, *Biopolymers*, 2004, **74**, 328–335.
28 G. Kister, G. Cassanas and M. Vert, *Polymers*, 1998, **39**, 267–273.
29 F. Ouyang, S. Yao, K. Tabata and E. Suzuki, *Appl. Surf. Sci.*, 2000, **158**, 28–31.
30 A. L. Goodman, L. M. Campus and K. T. Schroeder, *Energy Fuels*, 2004, **19**, 471–476.
31 Z. Zhang, M. F. Hossain, T. Miyazaki and T. Takahashi, *Environ. Sci. Technol.*, 2010, **44**, 4741.